Proceedings of ASME Turbo Expo 2021
Turbomachinery Technical Conference and Exposition
GT2021
June 7-11, 2021, Virtual, Online

GT2021-60074

PREDICTING THE AMPLITUDE OF THERMOACOUSTIC INSTABILITY USING UNIVERSAL SCALING BEHAVIOUR

Induja Pavithran*
Department of Physics
Indian Institute of Technology Madras
Chennai-600036, India

Vishnu R. Unni
Abhishek Saha
Department of Mechanical and Aerospace Engineering
University of California San Diego
California, CA-92093, US

Alan J. Varghese
R. I. Sujith
Department of Aerospace engineering
Indian Institute of Technology Madras
Chennai-600036, India

Norbert Marwan
Jürgen Kurths
Potsdam Institute for Climate Impact Research
14473, Potsdam, Germany

ABSTRACT

The complex interaction between the turbulent flow, combustion and the acoustic field in gas turbine engines often results in thermoacoustic instability that produces ruinously high-amplitude pressure oscillations. These self-sustained periodic oscillations may result in a sudden failure of engine components and associated electronics, and increased thermal and vibrational loads. Estimating the amplitude of the limit cycle oscillations (LCO) that are expected during thermoacoustic instability helps in devising strategies to mitigate and to limit the possible damages due to thermoacoustic instability. We propose two methodologies to estimate the amplitude using only the pressure measurements acquired during stable operation. First, we use the universal scaling relation of the amplitude of the dominant mode of oscillations with the Hurst exponent to predict the amplitude of the LCO. We also present a methodology to estimate the amplitudes of different modes of oscillations separately using 'spectral measures' which quantify the sharpening of peaks in the amplitude spectrum. The scaling relation enables us to predict the peak amplitude at thermoacoustic instability, given the data during the safe operating condition. The accuracy of prediction is tested for both methods, using the data acquired from a laboratory-scale turbulent combustor. The estimates are in good agreement with the actual amplitudes.

NOMENCLATURE

TAI Thermoacoustic instability
LCO Limit cycle oscillations
CN Combustion noise
INT Intermittency
p'_{rms} rms of pressure fluctuations
FFT peak Amplitude of the peak in the amplutude spectrum
H Hurst exponent
$[\mu_2\mu_0]$ Spectral measure
Re Reynolds number

*Address all correspondence to indujap2013@gmail.com

INTRODUCTION

Thermoacoustic instability is a severe problem faced by the propulsion and power industry [1]. Practical combustion applications such as gas turbine engines and rocket motors often encounter thermoacoustic instability. The occurrence of such instabilities has led to annual losses amounting to billions of dollars for power generation companies [2]. Thermoacoustic instability (TAI) manifests as high amplitude pressure oscillations that arise due to the establishment of a positive feedback mechanism between the acoustic field and the unsteady heat release rate. In a confined combustion system, this interaction between the subsystems, under appropriate conditions, can have catastrophic effects. The spontaneous emergence of such oscillations induces increased thermal and mechanical loading to the combustor, forcing a shut down of gas turbines or structural damage and reducing the life span of the combustor [2]; in rockets, it leads to even mission failures. Thus, there has been an increasing demand for methodologies to mitigate TAI.

One solution to mitigate TAI involves implementing control strategies to suppress these oscillations. In general, passive control strategies are preferred. The control mechanisms generally involve modifications of the combustor geometry, fuel injector geometry or microjet injection [3]. These strategies are implemented based on ad hoc modifications, investing a lot of money and time.

Alternately, there has been work on development of precursors to predict the proximity to TAI, methods to estimate the amplitude of TAI using the data acquired during stable operation, and implementing control strategies to suppress these oscillations. It would be desirable to perform the detection and control before the system reaches TAI rather than looking at the amplitude or root mean square (rms) of the fluctuations. There have been successful attempts to predict the onset of TAI. The stability margin was determined using several methods such as autocorrelation of the acquired pressure signal [4], exhaust flow and fuel injection rate modulation [5], etc.

Recently, researchers have developed techniques to determine stability boundaries based on only acoustic pressure measurements. During stable operation, acoustic pressure oscillations are chaotic [6, 7], and the loss of chaotic nature is quantified to obtain precursors [6]. Furthermore, Nair et al. [8] used the Hurst exponent to characterize the fractal nature of data during the transition to TAI. They showed that the variation of the Hurst exponent captures this transition well-before traditional measures. As another approach, recurrence quantification analysis has been used to provide precursors to TAI, by identifying the recurrences in the phase space reconstructed from the time series of acoustic pressure [9, 10]. The measures derived from complex networks are also used to provide precursors for such transitions [11,12]. There are many other methods to obtain early warning signals; these include the use of synchronization index, modified permutation entropy [13], etc. A few studies are available on precursors to TAI based on artificial intelligence (AI), and a combination of AI with physics-based precursors [14–16].

Being able to determine the amplitude during TAI helps to design appropriate control strategies. If the estimated amplitude is low enough that the combustor can handle it, then the combustor can be operated safely during TAI as well. However, if the amplitude is deemed dangerous for the combustor, either we can evade TAI or appropriate countermeasures such as increasing the flame length by using alternate fuel paths can be made.

Several studies have been conducted in the past to estimate the amplitude of limit cycle oscillations (LCO) during thermoacoustic instability. Traditionally, the amplitude is estimated utilizing flame describing functions (FDF) [17, 18]. FDF characterizes the linear or nonlinear response of flame to external perturbations of different amplitudes and frequencies. For better predictions, Krediet et al. [19] considered acoustic boundary losses along with the FDF, and the accuracy of the predictions could depend upon both the FDF and the acoustic losses [19].

Even though predicting the amplitude using FDF has been reported to be successful in many cases, forcing the system at high amplitudes to obtain FDF is costly and difficult for industrial engines. It is hard to design actuators to produce high amplitude oscillations, and exciting such high amplitudes in high pressure gas turbine combustors is not advisable. Recently, Seshadri et al. [20] proposed a methodology for predicting the amplitude based on intermittency statistics where TAI is associated with vortex shedding. They considered the acoustic field as a kicked oscillator and the impingement of a vortex carrying unburned reactant mixture results in a burst of heat release which, in turn, adds energy to the acoustic field. Then, an equation is derived for the slow-varying amplitude of oscillations from the reduced-order model for a combustion system with vortex shedding. They were able to predict the amplitude of LCO successfully for bluff body and swirl stabilized combustors.

Traditionally, thermoacoustic instability in combustion systems was considered as a transition from a stable fixed point to periodic oscillations as the control parameter is varied. Recently, Nair et al. [21] reported that the state of intermittency presages the transition to limit cycle oscillations in turbulent fluid mechanical systems. While studying the transition to TAI, the effects of turbulence are often considered as background noise and are neglected in the traditional approach. However, these irregular fluctuations are not just noise; in contrast, they are deterministic [7] and arise out of the turbulent dynamics. We treat these fluctuations with their inherent complexities as opposed to considering them as noise and quantify the fractal characteristics of the acoustic pressure fluctuations using a measure known as Hurst exponent (H). H describes how the rms of the standard deviation of fluctuations scales with the time over which it is calculated. While the amplitude of pressure fluctuations increases steeply near the onset of the TAI, H decreases smoothly and relatively much earlier than the rise in amplitude. The am-

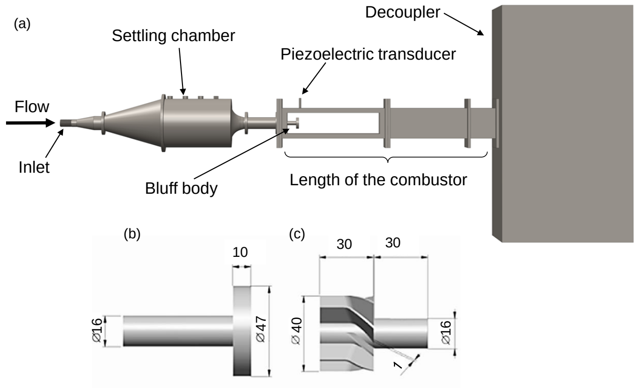

FIGURE 1. Schematic of the experimental set up for the turbulent combustor. The setup consists of a settling chamber, a burner, a flame holding mechanism and a combustion chamber with a variable duct length. We use two different flame holding mechanisms, a bluff body (shown in **b**) and a swirler (shown in **c**), attached to the burner by a central shaft. All dimensions are given in mm.

plitude of the dominant mode of oscillations follows an inverse square law scaling with the Hurst exponent [22]. In the current study, we use this concept to predict the amplitude of the LCO during TAI. Irrespective of the frequency of oscillations or the underlying physics of the problem, the data acquired from various configurations of thermoacoustic, aeroacoustic and aeroelastic systems obey this inverse square law. Hence, we estimate the amplitude of LCO by extrapolating the universal power law relation towards TAI (i.e., H tending to zero).

We also present a methodology to estimate the amplitudes of different modes of oscillations separately using 'spectral measures' which quantify the sharpening of peaks in the power spectrum. The spectral measures are calculated as the product of different moments of the normalized power spectrum raised to integer powers, and they follow inverse power law relations with the corresponding peak power [23]. Once we have the time series of acoustic pressure oscillations during the stable operation, we can generate the power spectrum and identify all the possible modes that are expected to grow. The scaling relation enables us to predict the amplitude during TAI, given the value of spectral measures and the amplitude at the safe operating condition. The objective of this study is to present the application of the patent-pending methodologies [24, 25] for predicting the amplitude of TAI.

In the rest of the paper, we first describe the experiments in the next section. Subsequently, we discuss the results which include characterizing the transition to TAI using the two methods and the interpretation of the inverse power laws. Then, we detail the procedure of estimation of amplitude and illustrate its efficacy using some examples.

EXPERIMENTS

The setup consists of a settling chamber, combustion chamber with flame holding mechanisms, ignition spark plug and a decoupler. Air enters through the inlet, and the fuel is injected through the central shaft holding the bluff body or swirler. The reactant mixture gets ignited using the ignition spark plug just before the combustion chamber. The length of the combustion chamber can be varied; in this study, we use lengths of 700 mm, 1100 mm and 1400 mm. We perform experiments with both bluff-body stabilized combustor and a swirl stabilized combustor. Liquified petroleum gas (LPG: butane 60 % and propane 40 % composition by mass) is the fuel used. Air is partially premixed with LPG for the experiments. We increase the Reynolds number (Re) by increasing the mass flow rate of air, and keeping the mass flow rate of fuel constant. The mass flow rates are controlled using mass flow controllers (Alicat MCR series) with an uncertainty of 0.8% of reading + 0.2% of full scale. The Reynolds number is calculated as $Re = 4\dot{m}D_1/\pi\mu D_0^2$, where $\dot{m}$ is the mass flow rate of air-fuel mixture, μ is the dynamic viscosity of the mixture, D_0 is the diameter of the burner and D_1 is the diameter of the bluff-body ($D_1 = D_0$ for swirler). The uncertainty in Re is calculated considering the uncertainty in the flow rates of air and fuel. More details of experiments including all the dimensions can be found in Nair & Sujith [8] and Nair et al. [21]. We use a piezoelectric transducer, PCB106B50, (sensitivity = 72.5 mV/kPa, resolution = 0.48 Pa and 0.64 % uncertainty) to measure the pressure fluctuations inside the combustion chamber. The sensor is mounted at the anti-node location of the acoustic oscillations to record the peak amplitude of the standing wave. The data is acquired at a sampling rate of 10 kHz.

RESULTS AND DISCUSSIONS

Transition from combustion noise to TAI

We focus on the transition from the state of combustion noise (CN) to TAI following an intermittency (INT) route in turbulent thermoacoustic systems. We vary the Reynolds number (Re) as the control parameter to study this transition. The time series of acoustic pressure fluctuations acquired at different values of Re during the transition are analyzed. Figure 2 shows three such time series and the corresponding amplitude spectra for the states of CN, INT and TAI. The time series during CN comprises low amplitude aperiodic oscillations which have deterministic chaotic characteristics [7]. Furthermore, these oscillations are multifractal [8] due to the presence of the underlying turbulent flow. As we approach TAI, we start to observe bursts of periodic oscillations in the data. A state of intermittency which consists of epochs of high amplitude periodic oscillations amidst low amplitude chaotic oscillations is present during the transition to TAI. The periodic content increases and becomes self-sustained limit cycle oscillations (LCO) during the state of full-blown instability. Along with this, the dominant peak in the amplitude

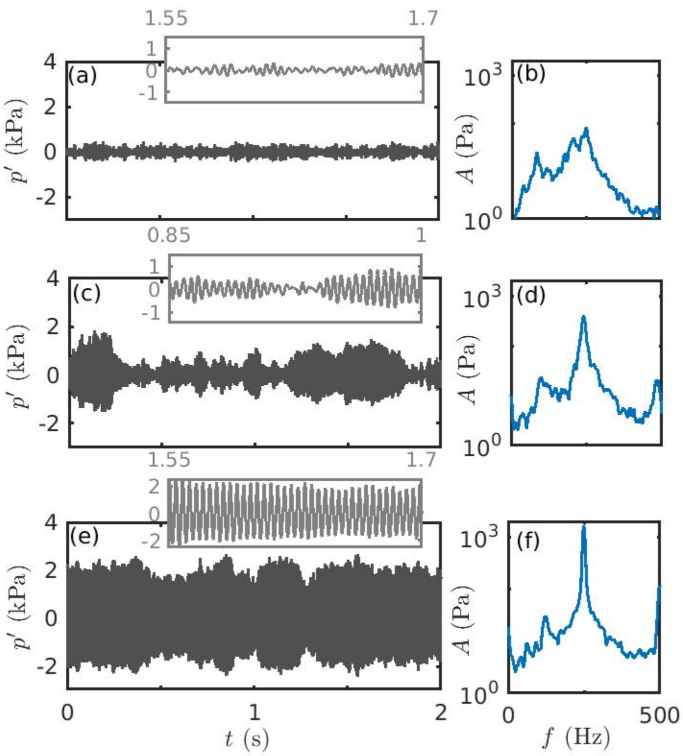

FIGURE 2. Time series and the corresponding amplitude spectrum of acoustic pressure fluctuations during the transition from CN to TAI. The data obtained for the bluff body stabilized combustor is presented here as a representative case; we observe a similar transition in swirl stabilized combustor as well. (**a**) The time series representing the state of CN ($Re = (1.9 \pm 0.053) \times 10^4$) consists of low amplitude aperiodic oscillations. (**b**) The amplitude spectrum shows a broad peak around $f = 250$ Hz. (**c**) We observe a state of INT at $Re = (2.6 \pm 0.069) \times 10^4$. The time series during INT has bursts of high amplitude periodic oscillations amidst epochs of low amplitude aperiodic oscillations. This reflects as an increase in the amplitude of the peak in the amplitude spectrum (**d**). Then, the amplitude of pressure fluctuations increases abruptly during TAI. (**e**) The time series during TAI (at $Re = (2.8 \pm 0.073) \times 10^4$) comprises high amplitude periodic oscillations and the resultant amplitude spectrum (**f**) has a sharp peak around $f = 250$ Hz.

spectrum changes from a broad peak to a sharp one.

Figure 3 shows the variation of p'_{rms} and the amplitude of dominant mode (FFT peak) as a function of Re. For relatively lower Re, both p'_{rms} and FFT peak are very low due to the presence of low amplitude aperiodic fluctuations during CN. We note that p'_{rms} is slightly greater than the FFT peak during CN, as the time series is aperiodic to a great extent and the energy is distributed over a wide range of frequencies. The FFT peak accounts for only the amplitude of the dominant mode. Hence, during TAI, we observe that the FFT peak becomes higher than p'_{rms} by a factor of $\sqrt{2}$ as expected for a sinusoidal signal because all the energy is being transferred to a single frequency. Also, the oscillations grow to a very high amplitude during TAI. We use Hann windowing while performing fast Fourier transform (FFT). The method of windowing helps to get a consistent estimation of the peak amplitude. We can minimize issues of spectral leakage by applying windowing. In this case, we use a Hann window for 0.25 s long data segments, thereby fixing a resolution of 4 Hz for the FFT. We find the FFT peak as the average of peak amplitudes of these 0.25 s windows for the full 3 s data.

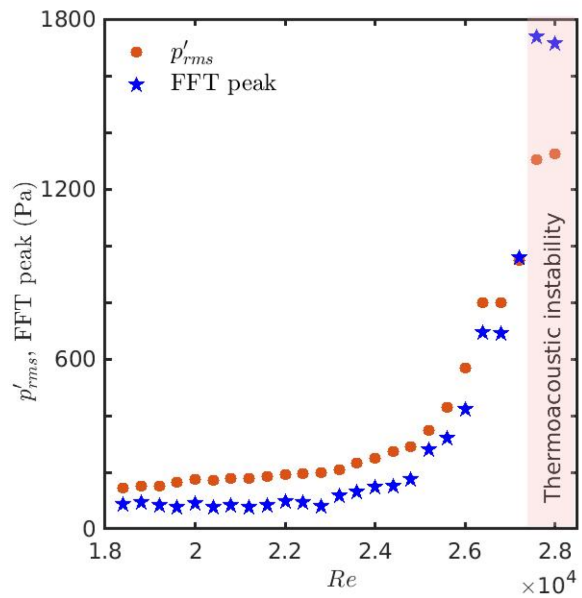

FIGURE 3. The variation of p'_{rms} and the FFT peak during the transition from CN to TAI. The amplitude of dominant mode of oscillations computed from the amplitude spectrum using the Fourier transform is referred to as the FFT peak. Both p'_{rms} and FFT peak are very low during CN. The amplitude of oscillations increases as we approach TAI, which is captured by both p'_{rms} and FFT peak. This figure uses data acquired from a bluff body stabilized turbulent combustor.

Fractal characteristics and universal scaling

To quantify the fractal characteristics of acoustic pressure fluctuations during the transition to TAI, we use the Hurst exponent (H). For a time series, H is related to the fractal dimension (D) as $H = 2 - D$. We calculate H following the procedure of Multifractal Detrended Fluctuation Analysis (MFDFA) [26]. In MFDFA, we first subtract the mean ($\bar{x}$) from the time series of length N, and calculate the cumulative deviate series $Y(k)$ as, $Y(k) = \sum_{t=1}^{k}[x_t - \bar{x}]$, where $k = 1, 2, ..., N$. Then, the deviate series $Y(k)$ is divided into non-overlapping segments of size w, and

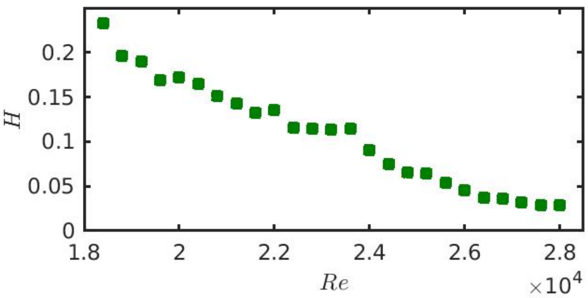

FIGURE 4. Variation of H as a function of Re for the acoustic pressure data from the bluff body stabilized combustor. H approaches a limiting value of zero for LCO, unlike amplitude which is unbounded and can increase to any level depending on the system.

the number of such segments, N_w is the greatest integer of N/w. To obtain the fluctuations, we subtract the polynomial fit from the deviate series (Y_i) for each segment i. The structure function of order 2 is defined as follows:

$$F_2(w) = \left[\frac{1}{N_w}\sum_{i=1}^{N_w}\left[\frac{1}{w}\sum_{t=1}^{w}(Y_i(t)-\bar{Y}_i)^2\right]\right]^{1/2}. \quad (1)$$

We calculate the structure function for different time scales w. The slope of the linear regime of the plot of variation of F_2 with the span w in a double logarithmic scale is known as the Hurst exponent (H).

H takes values between 0 and 1 for time series, corresponding to fractal dimension between 1 and 2. $H > 0.5$ indicates that the time series is a persistent one, *i.e.,* an increase (decrease) in the value of time series is likely to be followed by an increase (decrease) in its value. In contrast, an antipersistent signal would have $H < 0.5$, which is characterized by a decrease (increase) in the value is most likely to be followed by an increase (decrease) in its value and vice versa. An uncorrelated random process has $H = 0.5$. Unlike mathematical fractal objects, real fractal time series (experimental data) possess fractal nature only for a certain range of time scales. Hence, we need to select a range of scales that is optimal to capture the fractal characteristics during the transition. Here, we choose two to four acoustic cycles of oscillations of the natural frequency of the system [8, 27]. If we select scales with a length corresponding to less than one cycle of oscillation, then the periodicity in the data may not be captured. Also, the fluctuations are averaged out for long segments with a large number of cycles.

The aperiodic fluctuations observed during the state of CN has $H > 0.2$ (Fig. 4). As the periodic content in the signal increases during the transition, the fractal nature is lost. H captures this changing fractal characteristics, exhibiting a monotonic decrease in value tending towards zero. Moreover, the value of H is bounded. H decreases smoothly during the transition, while the FFT peak increases steeply near the onset of the TAI. The amplitude of the dominant mode of oscillations scales with the Hurst exponent following an inverse power law, $A_0 \propto H^{-2.0\pm0.2}$ (Fig. 5). We observe this scaling relation during the emergence of oscillatory instabilities from turbulence, in different configurations of thermoacoustic systems, aeroacoustic and aeroelastic systems [22]. The average power law exponent is -2±0.2 across these systems. We disregard the states with $H > 0.15$ as the tail of the power law; we observe the scaling approximately from $H < 0.15$. The tail of the power law consists of the states which are far from TAI.

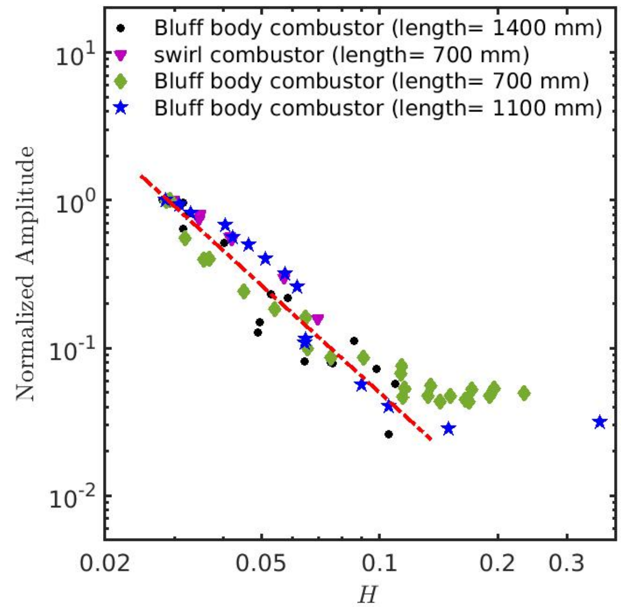

FIGURE 5. The inverse square law relation between H and FFT peak during the transition to TAI in turbulent systems. We present the scaling for the data acquired from the bluff body stabilized combustor with different lengths and a swirl stabilized combustor. As different configurations of the thermoacoustic system can have different amplitudes of LCO, we normalize the peak amplitude with the amplitude of LCO for that particular case. The normalization is done only for visualization purpose. A dashed red line is drawn to show the inverse power law.

Spectral measures to estimate the amplitude of individual modes of oscillations

The emergence of self-sustained periodic oscillations from an initially disordered state in various systems is accompanied by the phenomenon of spectral condensation, which is the narrow-

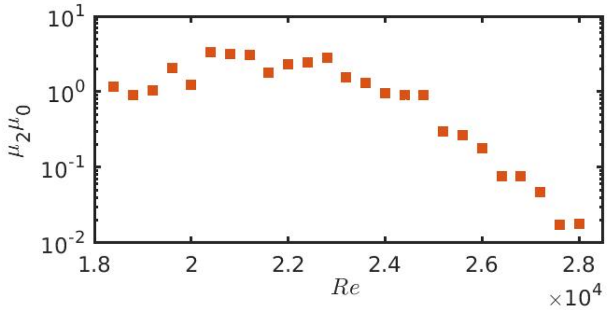

FIGURE 6. A representative spectral measure $[\mu_2\mu_0]$ as a function of *Re* in a semi logarithmic scale. The variation has a fluctuating trend during CN. However, the value of $[\mu_2\mu_0]$ decreases monotonically as we approach TAI.

ing of the peak in the amplitude spectrum accompanied by the growth of amplitude of the dominant oscillatory mode [23]. To quantify spectral condensation, Pavithran et al. [23] used spectral measures which are defined as the products of different moments of the power spectrum. They showed that the peaks in the power spectrum follow a power law scaling with these spectral measures.

In the present study, we aim to predict the amplitude of TAI using the scaling relation exhibited by the spectral measures. Therefore, we use the amplitude spectrum instead of the power spectrum, akin to the manner in which Pavithran et al. [23] used power spectrum to obtain a universal scaling relation. The spectral measures are denoted as $[\mu_m\mu_n]$, where μ_m is the m^{th} moment of the amplitude spectrum, and m & n are integers. Here, we use a representative spectral measure $[\mu_2\mu_0]$ (the product of 2^{nd} and 0^{th} moments) defined as,

$$[\mu_2\ \mu_0] = \left[\int_{-\delta F}^{+\delta F} \frac{A(F)}{A_0}\left|\frac{F}{f_0}\right|^2 dF\right] \times \left[\int_{-\delta F}^{+\delta F} \frac{A(F)}{A_0} dF\right], \quad (2)$$

where, $A(F)$ is the amplitude corresponding to the modified frequency $F = f - f_0$. Here, f is the variable indicating the frequency of oscillations, f_0 is the central frequency corresponding to the peak in the spectrum, and A_0 is the maximum amplitude at the center of the peak ($A(f_0)$). We calculate the spectral measure for the peak at f_0 in the neighbourhood of width δF (we use $\delta F \sim f_0/5$).

During the transition to TAI, the broad peak in the amplitude spectrum observed during CN sharpens to a narrow peak, while the amplitude grows. According to Eq. 2, the spectral measure $[\mu_2\mu_0]$ decreases as the peak becomes sharper. We present the variation of $[\mu_2\mu_0]$ in Fig. 6. During CN, the spectral measure does not decrease much and fluctuates near a constant value. Then, it starts to drop to a lower value as we approach TAI. We

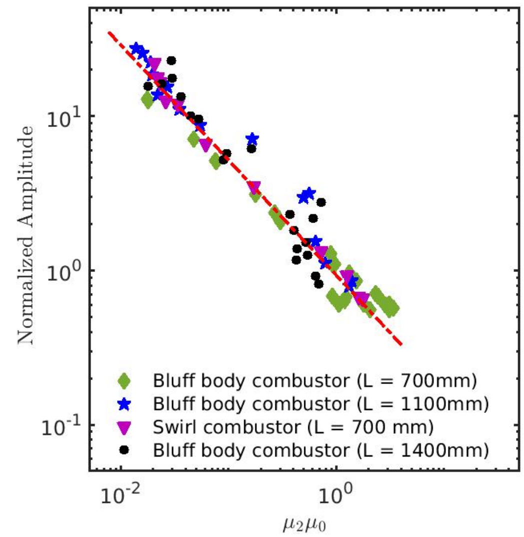

FIGURE 7. The inverse power law scaling between FFT peak and $[\mu_2\mu_0]$. The data acquired from the bluff body combustor with different lengths and the swirl combustor obey the power law relation with the same exponent. The FFT peak from the amplitude spectrum is normalized to show all these power laws in the same plot (for the sake of visualization). The normalization factor is the estimated value of FFT peak for $[\mu_2\mu_0]$ = 1 obtained by extrapolating power law for each system. The average value of the power law exponent across different systems including thermoacoustic, aeroacoustic and aeroelastic systems is found be around -0.66±0.1.

calculate the spectral measure for all the possible modes that are expected to grow. Thereby, we can track the growth of individual modes of oscillations. The spectral measure follows an inverse power law relation with the corresponding peak amplitude as, $A_0 \propto [\mu_2\mu_0]^{-0.66\pm0.1}$. We use this concept of universal scaling of the peak amplitude and spectral measure to estimate the amplitude of individual modes of oscillations. Note that the power law exponent obtained using the spectral measures defined on the amplitude spectrum with the Hann window is different from the power law exponent for spectral measures from the power spectrum [23].

Procedure to estimate the amplitude of limit cycle oscillations

These universal scaling relations during the transition to oscillatory instability are observed not just in thermoacoustic systems, but also in other fluid mechanical systems such as aeroacoustic and aeroelastic systems. Commonality among transitions in all these systems is that they exhibit emergence of ordered behavior from a background turbulent flow field following an inter-

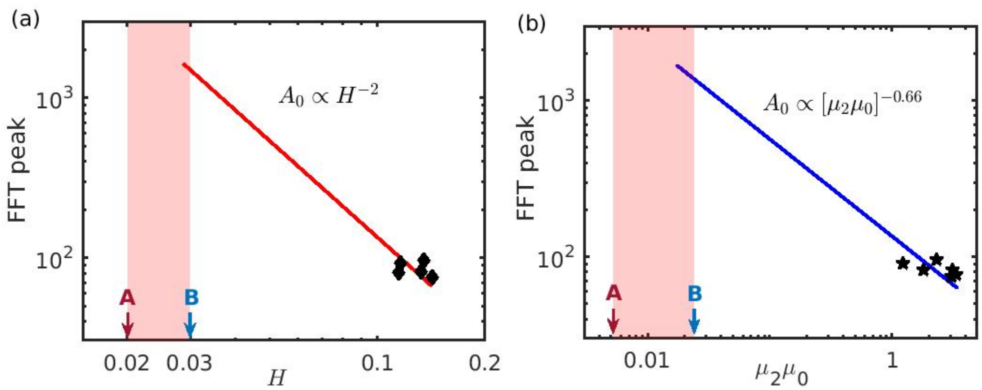

FIGURE 8. Estimating the amplitude of limit cycle oscillations using (**a**) the scaling of FFT peak and H and (**b**) the scaling of FFT peak and the spectral measure $[\mu_2\mu_0]$. We use a few data points during the state of stable operation (shown as black colour points) and extrapolate the power law behaviour towards TAI, that is towards higher FFT peak. The CN data shown here is obtained from the bluff body stabilized combustor of length 700 mm. The amplitudes in the region between A and B are the estimated amplitude during TAI.

mittency route. However, the underlying physical mechanisms involved in these systems are indeed different, suggesting that this scaling is characteristic of the underlying bifurcation in the system and is not determined by the specific physical processes that govern the system. The current manuscript aims to illustrate the method of amplitude estimation of the limit cycle oscillations using these scaling relations.

We describe the procedure of estimation of the amplitude of TAI using a few input data during stable operation. We plot the power law relations, $A_0 \propto H^{-2.0\pm0.2}$ and $A_0 \propto [\mu_2\mu_0]^{-0.66\pm0.1}$ passing through the points corresponding to the input data acquired during stable operation. We extrapolate the power laws towards TAI to find the y-intercept (refer Fig. 8). According to the definition of H and $[\mu_2\mu_0]$, we know that both reduce towards zero as we approach TAI. However, H and $[\mu_2\mu_0]$ will never attain the value of zero because of the discrete representation of the analog signal. We need the limiting values for H and $[\mu_2\mu_0]$ to estimate the amplitude of LCO. The theoretical value for H is 0 for a pure sine signal; however, for a limit cycle data acquired for a finite time duration, the lowest possible value would be around 0.02 (marked A in Fig. 8a). To fix the lowest limit for $[\mu_2\mu_0]$, we construct a unit amplitude sine wave with the same frequency as the natural frequency of the system and with the same sampling frequency as that of the experimental data. The value of $[\mu_2\mu_0]$ for this sine wave is the lower limit A (marked in Fig. 8b). The theoretical value of $[\mu_2\mu_0]$ for a sine wave according to Eq. 2 is 0. This would happen only if the amplitude spectrum is a Dirac delta function which has a nonzero amplitude only at f_0. However, the finite time interval for which the data is acquired attributes a nonzero width in the amplitude spectrum at f_0. This interplay between the localization in the time and frequency domain is in accordance with Heisenberg's uncertainty principle. In addition to this, we use a Hann window of 0.25 s length and the corresponding amplitude spectrum has a reduced resolution of 4 Hz. All these impose a nonzero limit on the value of the $[\mu_2\mu_0]$ for a sine wave.

The estimated amplitude for this limit A corresponds to the maximally "clean" periodic dynamics possible during TAI. For systems that exhibit a smooth transition to TAI via intermittency, this estimate will always be higher than the amplitudes that are practically attainable. A pure sine wave will not be achieved in turbulent systems. The estimated maximum amplitude (limit A) can be considered for designing the combustor. Now, we proceed to set an upper limit B for the threshold values of H and $[\mu_2\mu_0]$. Here, we construct a sine wave with amplitude modulations using the information from the time series of combustion noise. The periodic oscillations during TAI appear to have inter-cycle variability in amplitude, as shown in Fig. 2 (e). Lieuwen [28, 29] discussed the role of noise and system nonlinearities upon the temporal features of the limit-cycle pressure oscillations. Therefore, the limit B corresponds to a sine wave with a noisy amplitude envelope as observed during TAI in practical cases. We extract the envelope (E) of the acoustic pressure fluctuations acquired during CN using Hilbert transform [30]. Then, we construct a unit amplitude sine wave and modify its envelope with the extracted amplitude from the experimental data as $x(t) = (1 + E_{normalized}) sin\ \omega t$. The amplitude envelope is normalized ($E_{normalized} = (E–mean(E))/max(E)$), as we consider only its temporal characteristics.

Further, we can continuously improve the prediction by narrowing the range of estimated amplitudes between A & B, as we have more data points during the transition to TAI. When we estimate the amplitude using the data acquired during INT, the envelope of the signal is less noisy compared to that of CN and

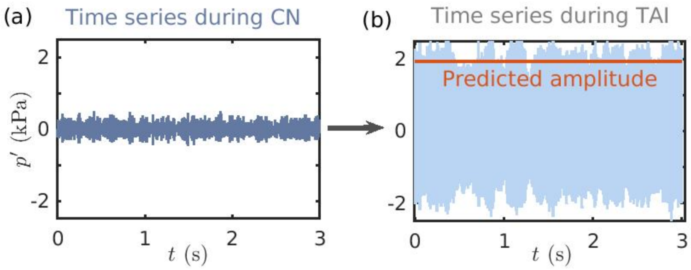

FIGURE 9. Time series showing aperiodic oscillations during stable operation at $Re = 1.95 \times 10^4$ and the time series with high amplitude limit cycle oscillations during TAI ($Re = 2.78 \times 10^4$). The predicted amplitude (using H), indicated with the red line, reasonably captures the actual limit cycle amplitude. The data presented is for the case of the bluff body stabilized combustor.

resembles experimental data more. As a result, the values of H and $[\mu_2\mu_0]$ corresponding to limit B reduce. Using the envelope of INT shifts limit B towards A. Hence, we can narrow the range of estimated amplitudes, as we have more data during intermittency. The shaded region in Fig. 8 corresponds to the predicted region of TAI. A more elaborate explanation on the method of selecting the limits A & B is given in Appendix A.

Illustration of efficacy of the estimation procedure

We need to test how well the estimation works when applied to experimental data obtained from practical thermoacoustic systems. We use pressure time series obtained from a bluff body and a swirl stabilized combustors having lengths 700 mm to illustrate the efficacy of the devised estimation technique. First, we take only one time series during CN and try to predict the amplitude of TAI. In Fig. 3, there are two data points in the region of TAI. In order to compare the predicted amplitude with the actual value, we find the H and $[\mu_2\mu_0]$ of the data corresponding to TAI, which are available from the experiments. Then, using the power law expression, we predict the amplitude corresponding to that particular values of H and $[\mu_2\mu_0]$, and we calculate the deviation of this predicted values from the actual amplitudes.

Subsequently, we try to predict using a higher number of time series data during the CN and INT. Such estimates are in good agreement with the actual values (Fig. 9). The predicted amplitudes and the error in prediction, using H and $[\mu_2\mu_0]$ are listed in Table 1 & 2. Each row in the table shows the results obtained using all the data in the preceding rows together. The actual amplitudes of LCO for bluff body and swirl stabilized combustors are 1737 Pa and 1509 Pa, respectively. For the bluff body case, the estimate obtained using three input time series is 1922 Pa and 1865 Pa using H and $[\mu_2\mu_0]$, respectively. Note that, these values are within 12% and 7% of the actual amplitude. The estimates using H and $[\mu_2\mu_0]$ for the swirl stabilized combustor have -5% and -20% deviation from the actual value. The accuracy of estimation using a single input time series depends on how well that particular data point fits to the power law scaling. Therefore, we can get significantly low errors in the estimate by using multiple input time series acquired during the transition. An in-

TABLE 1. Estimated amplitude of limit-cycle oscillations using the scaling relation of H and FFT peak from the time series acquired during the stable operation. The first row in the table shows the results from only one time series. The second row shows the results using the first and the second time series, and so on.

Re	FFT Peak	H	$A_{predicted}$	$\Delta A, \%$
1) Bluff body (Actual limit cycle amplitude = 1737 Pa)				
2.12×10^4	75.32	0.142	1864	9
2.16×10^4	82.22	0.132	1807	6
2.20×10^4	95.97	0.135	1922	12
2) Swirl (Actual limit cycle amplitude = 1509 Pa)				
1.35×10^4	139.64	0.129	1658	10
1.41×10^4	567.29	0.057	1325	-12
1.46×10^4	1119.97	0.043	1440	-5

TABLE 2. Estimated amplitude of limit-cycle oscillations using the scaling relation of spectral measure and FFT peak from the time series acquired during the stable operation.

Re	FFT Peak	$[\mu_2\mu_0]$	$A_{predicted}$	$\Delta A, \%$
1) Bluff body (Actual limit cycle amplitude = 1737 Pa)				
2.00×10^4	90.84	1.23	1506	-13
2.04×10^4	77.23	3.39	1712	-2
2.08×10^4	82.32	3.12	1865	7
2) Swirl (Actual limit cycle amplitude = 1509 Pa)				
1.35×10^4	139.64	0.37	1007	-33
1.41×10^4	567.29	0.05	1052	-30
1.46×10^4	1119.97	0.02	1212	-20

put time series, and the LCO along with the predicted amplitude (indicated with a red line) are shown in Fig. 9. The predicted value is indeed close to the actual amplitude of LCO. Note that the methods discussed in this paper are valid for highly turbulent systems which exhibit a steep, albeit smooth transition to TAI via INT. However, it is not clear whether such an approach will work if there is an abrupt jump in the amplitude at the onset of TAI. Further work needs to be done to estimate the amplitude of TAI under such conditions.

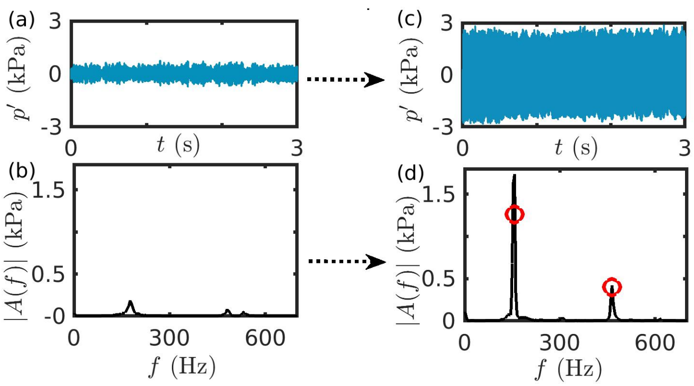

FIGURE 10. (a) low amplitude aperiodic p' during CN and (b) the corresponding amplitude spectrum with two broad peaks around 160 Hz and 500 Hz. (c-d) Both the modes grow as we reach TAI, and the peak at ∼158 Hz becomes dominant. The predicted amplitudes of these two modes are marked with red circles in the spectrum.

Estimating the amplitude of multiple modes of oscillations: We extend the method to predict the amplitude of individual modes of oscillations in thermoacoustics systems, exhibiting multiple modes of oscillations. The experimental setup shown in Fig. 1 is observed to have thermoacoustics instability with a single frequency. However, the combustor with a preheater arrangement (to preheat the reactants) is found to excite different frequencies at different temperatures. Refer Pawar et al. [31] for more details of the experiments with preheater setup. We use the pressure data acquired at a preheat temperature of 300^0C. Figure 10 shows the time series and the amplitude spectra during CN and TAI. At this temperature, the peak at 158 Hz and 456 Hz become sharper during TAI. The dominant mode during TAI is 158 Hz (amplitude increases from ∼100 Pa to ∼1734 Pa). Also, the amplitude of the peak at 456 Hz increases from ∼80 Pa to ∼418 Pa, during the transition.

We calculate the $[\mu_2\mu_0]$ in the neighbourhood of both the peaks (f_1 = 158 Hz and f_2 = 456 Hz) and estimate the amplitude using the scaling relation $A \propto [\mu_2\mu_0]^{-0.66}$. The estimated peak amplitude values using 3 pressure time series data during CN is

TABLE 3. Estimation results for data with multiple modes

Re	FFT peak	$[\mu_2\mu_0]$	$A_{predicted}$	$\Delta A, \%$
1) First mode, f_1 = 158 Hz (Actual amplitude = 1734 Pa)				
1.81×10^4	146.45	3.68	1236	-29
1.83×10^4	139.71	4.11	1250	-27
1.84×10^4	113.43	5.84	1261	-27
2) Third mode, f_2 = 456 Hz (Actual amplitude = 418 Pa)				
1.81×10^4	88.06	0.36	390	-6
1.83×10^4	105.80	0.26	381	-9
1.84×10^4	96.78	0.41	403	-4

marked with red colour circles in Fig. 10b. Further, the estimated values using a single time series and multiple time series data are listed in Table 3. When we compare the predicted and the actual values, the estimates for the first and second peak are within 30% and 10% error, respectively. Thus, the methodology using spectral measure can be applied to predict the amplitude of individual modes during TAI.

For the data from the combustor with preheater (with multiple modes), there is a significant error in the estimated amplitude calculated using the scaling of H. The possible reasons for this inaccuracy could be the low levels of turbulence present in the system and the presence of multiple peaks in the amplitude spectrum. Unlike the scaling of $[\mu_2\mu_0]$, the scaling with H is observed only in turbulent fluid mechanical systems. Further, the presence of peaks other than the dominant modes in the amplitude spectrum can effect the value of H since it is calculated over a certain range of time scales. Nevertheless, the variation of H during the transition provides indication of the impending TAI well in advance, and H can be used as a precursor. Further studies need to be done to identify the exact reason for the inaccuracy in amplitude estimation.

In this study, we showed the method of amplitude prediction for longitudinal modes. However, many practical combustors seldom show a single dominant frequency and often exhibit multiple frequencies. Further, the mode of instabilities can also be transverse (or azimuthal) or a combination of transverse and longitudinal modes. In the future, a detailed study for the performance of Hurst exponent and spectral measure towards early warning and amplitude estimation for such modes needs to be done. Further, multiple experiments in different configurations of the experimental setup with changes in different control parameters to approach thermoacoustic instability need to be conducted to establish more accurate error bars for the power law exponent. In the future studies, we aim to derive a theoretical framework for studying spectral condensation.

CONCLUSIONS

In this study, we present two different methods to predict the amplitude during thermoacoustic instability, by using time series data during the state of stable operation or intermittency. First, we show that the universal scaling relation between the amplitude of the dominant mode and the Hurst exponent in the intermittency regime can be exploited to predict the amplitude during TAI. We demonstrate that this method can predict the amplitude fairly accurately in practical systems, by applying this procedure to the data from a bluff body and a swirl stabilized combustor. However, in the case of a combustor with a preheater that exhibits multiple modes of oscillations, there is a significant error in the predicted amplitude. We speculate that this inaccuracy is due to the low levels of turbulence present and due to the presence of multiple peaks in the amplitude spectrum. Further studies need to be done to pinpoint the exact reason for this inaccuracy.

Along with this, we also show that the amplitude during TAI can be predicted by using the scaling relation between the amplitude of the dominant mode and the spectral measure. For this method as well, we show that the predictions are fairly accurate for the bluff body and swirl combustor. Interestingly, using this method, we are able to predict the amplitude of different modes of oscillations in the case of the combustor with a preheater. To improve the predictions, we need to perform more experiments with combustors exhibiting multiple frequencies.

Both these methods can be used by manufacturers of industrial gas turbines to estimate the amplitude during TAI, even without approaching anywhere close to instability. In other words, the amplitude can be estimated without exposing the combustor to large amplitudes and thereby endangering it. In the future, we would most probably see artificial intelligence based methods or a combination of AI with physics-based methods such as that presented here to predict the amplitude during TAI. AI based models are heavily used for the purpose of forecasting, especially for financial and weather data, currently. Such methods, when applied to thermoacoustics, in combination with physics based approaches such as that presented here, would hopefully give us more powerful tools to predict the amplitude during thermoacoustic instability.

ACKNOWLEDGMENT

We acknowledge the funding from the Department of Science and Technology, Government of India (Swarnajayanti Fellowship, grant Nos.: DST/SF/1(EC)/2006 and JCB/2018/000034/SSC - JC Bose Fellowship). We also thank Dr. V. Nair (IIT Bombay), Dr. G. Thampi (CUSAT), Dr. S. A. Pawar (IIT Madras) and our colleagues from the IIT Madras for the useful discussions. I.P. is thankful to Ministry of Human Resource Development, India and Indian Institute of Technology Madras for the research assistantship.

REFERENCES

[1] Juniper, M. P., and Sujith, R. I., 2018. "Sensitivity and nonlinearity of thermoacoustic oscillations". *Annual Review of Fluid Mechanics,* ***50***, pp. 661–689. DOI:10.1146/annurev-fluid-122316-045125.

[2] Lieuwen, T. C., and Yang, V., 2005. *Combustion instabilities in gas turbine engines: operational experience, fundamental mechanisms, and modeling*. American Institute of Aeronautics and Astronautics. DOI:10.2514/4.866807.

[3] Schadow, K., and Gutmark, E., 1992. "Combustion instability related to vortex shedding in dump combustors and their passive control". *Progress in Energy and Combustion Science,* ***18***(2), pp. 117–132. DOI:10.1016/0360-1285(92)90020-2.

[4] Lieuwen, T., 2005. "Online combustor stability margin assessment using dynamic pressure data". *J. Eng. Gas Turbines Power,* ***127***(3), pp. 478–482. DOI:10.1115/1.1850493.

[5] Johnson, C. E., Neumeier, Y., Lieuwen, T. C., and Zinn, B. T., 2000. "Experimental determination of the stability margin of a combustor using exhaust flow and fuel injection rate modulations". *Proceedings of the Combustion Institute,* ***28***(1), pp. 757–763. DOI:10.1016/S0082-0784(00)80278-7.

[6] Nair, V., Thampi, G., Karuppusamy, S., Gopalan, S., and Sujith, R. I., 2013. "Loss of chaos in combustion noise as a precursor of impending combustion instability". *International journal of spray and combustion dynamics,* ***5***(4), pp. 273–290. DOI:10.1260/1756-8277.5.4.273.

[7] Tony, J., Gopalakrishnan, E. A., Sreelekha, E., and Sujith, R. I., 2015. "Detecting deterministic nature of pressure measurements from a turbulent combustor". *Physical Review E,* ***92***(6), p. 062902. DOI: 10.1103/PhysRevE.92.062902.

[8] Nair, V., and Sujith, R. I., 2014. "Multifractality in combustion noise: predicting an impending combustion instability". *Journal of Fluid Mechanics,* ***747***, pp. 635–655. DOI: 10.1017/jfm.2014.171.

[9] Nair, V., Thampi, G., and Sujith, R. I., 2014. "Engineering precursors to forewarn the onset of an impending combustion instability". In Turbo Expo: Power for Land, Sea, and Air, Vol. 45691, American Society of Mechanical Engineers, p. V04BT04A005. DOI:10.1115/GT2014-26020.

[10] Gotoda, H., Shinoda, Y., Kobayashi, M., Okuno, Y., and Tachibana, S., 2014. "Detection and control of combustion instability based on the concept of dynamical sys-

tem theory". *Physical Review E,* ***89***(2), p. 022910. DOI:10.1103/PhysRevE.89.022910.

[11] Godavarthi, V., Pawar, S. A., Unni, V. R., Sujith, R. I., Marwan, N., and Kurths, J., 2018. "Coupled interaction between unsteady flame dynamics and acoustic field in a turbulent combustor". *Chaos: An Interdisciplinary Journal of Nonlinear Science,* ***28***(11), p. 113111. DOI:10.1063/1.5052210.

[12] Murugesan, M., and Sujith, R. I., 2016. "Detecting the onset of an impending thermoacoustic instability using complex networks". *Journal of Propulsion and Power,* ***32***(3), pp. 707–712. DOI:10.2514/1.B35914.

[13] Gotoda, H., Amano, M., Miyano, T., Ikawa, T., Maki, K., and Tachibana, S., 2012. "Characterization of complexities in combustion instability in a lean premixed gas-turbine model combustor". *Chaos: An Interdisciplinary Journal of Nonlinear Science,* ***22***(4), p. 043128. DOI:10.1063/1.4766589.

[14] Kobayashi, T., Murayama, S., Hachijo, T., and Gotoda, H., 2019. "Early detection of thermoacoustic combustion instability using a methodology combining complex networks and machine learning". *Physical Review Applied,* ***11***(6), p. 064034. DOI:10.1103/PhysRevApplied.11.064034.

[15] Hachijo, T., Masuda, S., Kurosaka, T., and Gotoda, H., 2019. "Early detection of thermoacoustic combustion oscillations using a methodology combining statistical complexity and machine learning". *Chaos: An Interdisciplinary Journal of Nonlinear Science,* ***29***(10), p. 103123. DOI:10.1063/1.5120815.

[16] Bhattacharya, C., O'Connor, J., and Ray, A., 2020. "Data-driven detection and early prediction of thermoacoustic instability in a multi-nozzle combustor". *Combustion Science and Technology*, pp. 1–32. DOI:10.1080/00102202.2020.1820495.

[17] Ćosić, B., Moeck, J. P., and Paschereit, C. O., 2013. "Prediction of pressure amplitudes of self-excited thermoacoustic instabilities for a partially premixed swirl-flame". In Turbo Expo: Power for Land, Sea, and Air, Vol. 55102, American Society of Mechanical Engineers, p. V01AT04A007. DOI:10.1115/GT2013-94160.

[18] Stow, S. R., and Dowling, A. P., 2004. "Low-order modelling of thermoacoustic limit cycles". In Turbo Expo: Power for Land, Sea, and Air, Vol. 41669, pp. 775–786. DOI:10.1115/GT2004-54245.

[19] Krediet, H., Krebs, W., Portillo, J. E., and Kok, J., 2010. "Prediction of thermoacoustic limit cycles during premixed combustion using the modified galerkin approach". In 46th AIAA/ASME/SAE/ASEE Joint Propulsion Conference & Exhibit, p. 7150. DOI:10.2514/6.2010-7150.

[20] Seshadri, A., Pavithran, I., Unni, V. R., and Sujith, R. I., 2018. "Predicting the amplitude of limit-cycle oscillations in thermoacoustic systems with vortex shedding". *AIAA Journal,* ***56***(9), pp. 3507–3514. DOI:10.2514/1.J056926.

[21] Nair, V., Thampi, G., and Sujith, R., 2014. "Intermittency route to thermoacoustic instability in turbulent combustors". *Journal of Fluid Mechanics,* ***756***, p. 470–487. DOI: 10.1017/jfm.2014.468.

[22] Pavithran, I., Unni, V. R., Varghese, A. J., Sujith, R. I., Saha, A., Marwan, N., and Kurths, J., 2020. "Universality in the emergence of oscillatory instabilities in turbulent flows". *EPL (Europhysics Letters),* ***129***(2), p. 24004. DOI:10.1209/0295-5075/129/24004.

[23] Pavithran, I., Unni, V. R., Varghese, A. J., Premraj, D., Sujith, R. I., Vijayan, C., Saha, A., Marwan, N., and Kurths, J., 2020. "Universality in spectral condensation". *Sci Rep 10, 17405*. DOI:/10.1038/s41598-020-73956-7.

[24] Pavithran, I., Unni, V. R., and Sujith, R. I., 2018. Patent of addition to the patent, system and method for predetermining the onset of impending oscillatory instabilities in practical devices - US9804054B2, Priority date: 23 Jul 2018.

[25] Pavithran, I., Unni, V. R., Varghese, A. J., Kasthuri, P., and Sujith, R. I., 2018. System and method for determining oscillatory instabilities in fluid mechanical devices - WO2020021565A1. India Provisional Patent Reference Number: 201841027977, Priority date: 25 Jul 2018.

[26] Ihlen, E. A. F. E., 2012. "Introduction to multifractal detrended fluctuation analysis in matlab". *Frontiers in physiology,* ***3***, p. 141. DOI:10.3389/fphys.2012.00141.

[27] Kerres, B., Nair, V., Cronhjort, A., and Mihaescu, M., 2016. "Analysis of the turbocharger compressor surge margin using a hurst-exponent-based criterion". *SAE International Journal of Engines,* ***9***(3), pp. 1795–1806. DOI:10.4271/2016-01-1027.

[28] Lieuwen, T. C., 2002. "Experimental investigation of limit-cycle oscillations in an unstable gas turbine combustor". *Journal of Propulsion and Power,* ***18***(1), pp. 61–67.

[29] Lieuwen, T. C., 2003. "Statistical characteristics of pressure oscillations in a premixed combustor". *Journal of Sound and Vibration,* ***260***(1), pp. 3–17.

[30] Panter, P. F., 1965. "Modulation, noise and spectral analysis: applied to information transmission".

[31] Pawar, S. A., Raghunathan, M., Reeja, K. V., Midhun, P. R., and Sujith, R. I., 2020. "Effect of preheating of the reactants on the transition to thermoacoustic instability in a bluff-body stabilized dump combustor". *Proceedings of the Combustion Institute*. DOI:10.1016/j.proci.2020.06.370.

Appendix A: Selecting the limits A and B

By definition, both H and the spectral measure $[\mu_2\mu_0]$ reduce towards zero as we approach TAI. However, H and $[\mu_2\mu_0]$ will never attain the value of zero because of the discrete representation of the analog signal. To estimate the lower limit of H and $[\mu_2\mu_0]$ in practical scenarios, we construct a unit amplitude si-

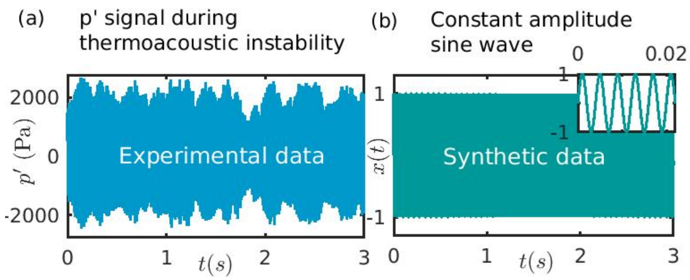

FIGURE 11. (a) A typical time series representing pressure fluctuations acquired from experiments during TAI and (b) a synthetic sine wave signal. The zoomed view shows the periodic nature of the signal.

nusoidal signal with the same frequency as the natural frequency of the system and with the same sampling frequency as that of the experimental data. Such a constant amplitude sine wave is representative of the maximally "clean" periodic dynamics possible during thermoacoustic instability. The H and spectral measure for this sinusoidal signal are considered as limit A in Fig. 8. Thus, the estimated amplitude corresponding to limit A is the maximum possible amplitude for a given system configuration.

Figure 11(a)-(b) shows the time series of pressure fluctuations acquired from the experiments during TAI and a synthetic sine wave signal with the same frequency, respectively. In contrast to the regularity in a clean sinusoidal signal, experimental data of pressure fluctuations during TAI have inter-cycle variability in the amplitude. The values of H and $[\mu_2\mu_0]$ for a clean sine wave will be close to zero, and the estimated amplitude will be higher than practically attainable amplitudes in highly turbulent systems exhibiting smooth transition via intermittency.

To avoid such an over-estimation of amplitude using limit A, we construct a sine wave with amplitude modulations to define limit B. We do not add any noise to get the envelope fluctuations; rather we use characteristics of time series data during stable operation. We extract the envelope (E) of the pressure fluctuations during CN using the Hilbert transform. Then, we construct a unit amplitude sine wave ($sin\ \omega t$) and multiply it with $(1+E_{normalized})$ as follows, $x(t) = (1+E_{normalized})sin\ \omega t$. Here, $E_{normalized} = (E – mean(E))/max(E)$.

Figure 12(a) shows three representative time series (I, II & III) acquired from the experiments (before the onset of TAI). The extracted envelope (E) is shown with a violet color. These envelopes are normalized as mentioned before and used to modify the sine waves. The time series in each row I, II, & III of Fig. 12(b) corresponds to the sine waves multiplied with the extracted envelopes from Fig. 12(a). The zoomed plot (Fig. 12(c)) shows that the signal is sinusoidal with amplitude modulations.

In Fig. 12(a), the time series I & II represents CN, and III corresponds to INT. From Fig. 12(b)I-III, we observe that the signal's envelope becomes less noisy (see the black curves indicating the envelopes of the sine waves). The signal in III b resembles the experimental data more than I b. The values of H and $[\mu_2\mu_0]$ for the sine waves with the envelope extracted from the three representative time series I, II & III are shown in Fig. 12(d). As expected, the values of H and $[\mu_2\mu_0]$ for the sine wave with the envelope of INT (Fig. 12(b)-III) are slightly lower than that of the case with combustion noise. Using the signal with the lower H and $[\mu_2\mu_0]$ shifts the limit B towards limit A (i.e., the difference between the two limits is reduced). Hence, we can narrow the range of estimated amplitudes (between A and B) by using the data for intermittency instead of combustion noise to extract the amplitude envelope.

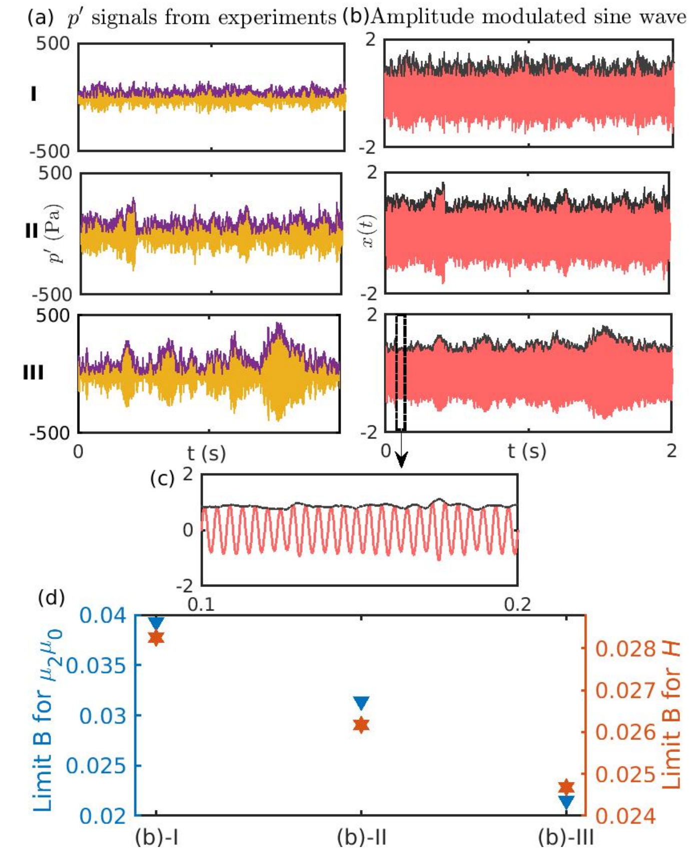

FIGURE 12. (a) Time series showing acoustic pressure signals during the states of stable operation. Three representative signals I, II & III are shown along with the extracted amplitude envelope. (b) Amplitude modulated sinusoidal signals with the envelope of experimental data shown in (a). The time series I - III are acquired during the transition towards TAI; I & II represent CN, and III corresponds to INT. From I - III (b), we observe that the envelope of the signal becomes less noisy. The zoomed plot (c) shows that the signal is sinusoidal with slight amplitude variations. The limit B evaluated for H and $[\mu_2\mu_0]$ for the signals in (b) are shown in (d).